A label-free ultrasensitive microfluidic surface Plasmon resonance biosensor for Aflatoxin B1 detection using nanoparticles integrated gold chip

Hema Bhardwaj, Gajjala Sumana, Christophe Marquette

Journal Pre-proofs

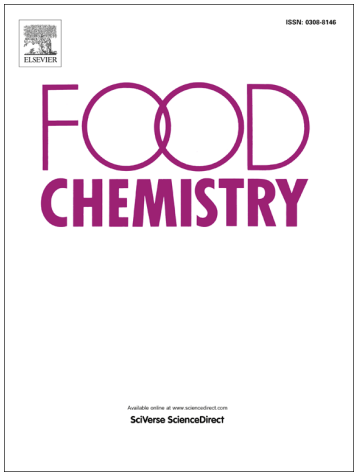

A Label-Free Ultrasensitive Microfluidic Surface Plasmon Resonance Biosensor for Aflatoxin B_1 detection using Nanoparticles integrated Gold chip

Hema Bhardwaj, Gajjala Sumana, Christophe A. Marquette

PII: S0308-8146(19)31649-8
DOI: https://doi.org/10.1016/j.foodchem.2019.125530
Reference: FOCH 125530

To appear in: *Food Chemistry*

Received Date: 24 May 2019
Revised Date: 6 September 2019
Accepted Date: 12 September 2019

Please cite this article as: Bhardwaj, H., Sumana, G., Marquette, C.A., A Label-Free Ultrasensitive Microfluidic Surface Plasmon Resonance Biosensor for Aflatoxin B_1 detection using Nanoparticles integrated Gold chip, *Food Chemistry* (2019), doi: https://doi.org/10.1016/j.foodchem.2019.125530

A Label-Free Ultrasensitive Microfluidic Surface Plasmon Resonance Biosensor for Aflatoxin B_1 detection using Nanoparticles integrated Gold chip

Hema Bhardwaj[a,b,c], Gajjala Sumana[b,c], Christophe A. Marquette[a*]

[a]Institute for Molecular and Supramolecular Chemistry and Biochemistry (ICBMS), University Claude Bernard Lyon 1, Villeurbanne Cedex-69100, France
[b]Academy of Scientific and Innovative Research (AcSIR), Ghaziabad-201002, India
[c]Biomedical Metrology Section, CSIR-National Physical Laboratory, Dr. K.S. Krishnan Marg, New Delhi-110012, India

Abstract

The Surface Plasmon resonance (SPR) based label-free detection of small targeted molecules is a great challenge and require substantial signal amplification for the accurate and precise quantification. The incorporation of noble metal nanoparticles (NPs) like gold (Au) NPs for the fabrication of SPR biosensor has shown remarkable impact both for anchoring the signal amplification and generate plasmonic resonant coupling between NPs and chip surface. In this work, we present comparative studies related to the fabrication of self-assembled monolayer (SAM) and the influence of AuNPs on Au chip for Aflatoxin B_1 (AFB_1) detection using SPRi apparatus. The SAM Au chip was sequentially modified by EDC-NHS crosslinkers, grafting of protein-A and finally interaction with anti-AFB_1 antibodies. Similar multilayer chip surface was prepared using functionalized lipoic acid AuNPs deposited on SAM Au chips followed by *in-situ* activation of functional groups using EDC-NHS crosslinkers, grafting of protein-A and immobilization of anti-AFB_1 antibodies. This multilayer functionalized AuNPs modified Au chip was successfully utilized for AFB_1 detection ranging from 0.01 to 50 nM with a limit of detection of 0.003 nM. When compared to bare self-assembled Au chip which was shown to exhibit a limit of detection of 0.19 nM and a linear detection ranging from 1 to 50 nM, the AuNPs modified Au chip was proven to clearly be a better analytical tool. Finally, validation of the proposed biosensor was evaluated by spiked wheat samples and average recoveries (93 and 90.1%) were found to be acceptable.

Keywords: Self-assembled monolayer, Gold nanoparticles, Protein-A, Aflatoxin B_1, Surface Plasmon Resonance, Biosensor

*Corresponding author: Email ID: christophe.marquette@univ-lyon1.fr (C.A. Marquette).

1. Introduction

The natural occurrence of mycotoxins in food and feedstuff is a major issue across the world which can cause severe health problems in humans, animals and other livestock (Richard et al., 2007). Mycotoxins are toxic fungal secondary metabolites produced by various fungi and moulds, particularly *Aspergillus, Fusarium, and Penicillium* (Goyal et al., 2016). It has been estimated that about 25% of the world's food crops every year get contaminated by mycotoxins, resulting in huge industrial and agricultural loss per year (Mateo et al., 2018). Among the various mycotoxins, AFB_1, which is a low molecular mass compound produced by *Aspergillus Flavus* and *Aspergillus Parasiticus,* is considered to be a potent, strong teratogen, mutagen, and carcinogen. AFB_1 is commonly found in various food and feedstuffs including cereals, oilseeds, spices, coffee beans, and nuts (Omrani et al., 2016, Negash et al., 2018). AFB_1 is classified by the International Agency for Research on Cancer (IARC) as a Group-1 Carcinogen that shows a high risk for Hepatocellular Carcinoma (Kensler et al., 2018). The European Commission has set a maximum permissible level of AFB_1 in food content to 5-10 μg/kg (Heshmati et al., 2017). Conventional, well-equipped laboratory techniques, such as high-performance liquid chromatography (HPLC) and thin layer chromatography (TLC) are commonly used for aflatoxins detection but usually lack sensitivity and sensibility (high limit of detection) (Wang et al., 2019). Advanced and more complex techniques also exist such as enzyme-linked immunosorbent assays (ELISA) and polymerase chain reaction (PCR) based assays which usually show higher sensitivity and sensibility but suffer cross-reactivity issues and difficulties of implementation for routine analysis (Koedrith et al., 2015).

In the past two decades, optical biosensors based on SPR appeared to be one of the most powerful technique for interaction kinetic analysis and label-free quantification of small biomolecules (<1000 Da) (Mullett et al., 2000, Nikolovska-coleska et al., 2015). Thus, SPR based biosensors have gained great attention in recent years due to their application in various areas such as biotechnology and life science research, agro-food analysis, environmental monitoring and medical diagnostics (Jia et al., 2018, Zhang et al., 2014).

In real-time monitoring, signal amplification for label-free detection of small molecules such as AFB_1 is a real challenge. However, only seldom efforts have been devoted to improving biosensing characteristics such as sensitivity and limit of detection for SPR based AFB_1 detection. Upon these few examples, Sun et al. proposed an SPR aptamer-based assay for AFB_1 detection ranging from 0.4 to 200 nM, with a limit of detection of 0.4 nM

(Sun et al., 2017). Recently, Park et al. developed bifunctional protein crosslinker-based SPR biosensor to detect AFB_1 where the genetically engineered fusion of gold binding protein and protein-G has been used to fabricate gold sensor chip. The limit of detection was 1 µg/mL in the detection range from 0.5 to 100 µg/mL (Park et al., 2014).

Noble metal NPs have also been used to enhance SPR signal response, leading to the enhancement of specificity and sensitivity for small biomolecules detection. Among the various described metallic NPs, spherical AuNPs are the most favorable for biosensing amplification thanks to their plasmonic properties, large dielectric constant, high surface-to-volume ratio and surface energy. Moreover, their isotropic structure allows the strong optical coupling to occur in every direction with incident light rather than to take place only in one direction, thereby enhancing the sensitivity of the SPR biosensor (Devi et al., 2015, Martinsson et al., 2014, Szunerits et al., 2014). Interestingly, AuNPs surface modification using suitable capping agents or ligands can provide functionality for bio-recognition elements immobilization. In this work, surface functionalization of AuNPs was modified by solvent extraction-based ligand exchange method, slightly modified from a literature reported method (Dewi et al., 2014). Briefly, the two-step process was utilized to complete the replacement of Cetyltrimethylammonium bromide (CTAB) surfactant to lipoic acid by maintaining their colloidal stability in an aqueous solution. In the first step, CTAB surfactant was partially removed from the aqueous phase of AuNPs to immiscible organic solvent of dichloromethane. Second, complete replacement of CTAB to lipoic acid was achieved through direct chemisorption, resulting in a higher degree of exchange. This approach is a versatile method for AuNPs surface modification also preserving colloidal stability, shape, and size of the particles.

Another important parameter for SPR biosensing performance is the quality of the bio-recognition element immobilization onto the sensor surface. Indeed, direct and random immobilization of antibodies on a solid sensing surface can generate antibodies conformational changes, leading to instability or loss of antigen-binding (Tsekenis et al., 2019). The immobilization of antibody binding protein such as protein-A which specifically bind with Fc region of an antibody without any chemical modification is one of the smart approaches leading to the immobilization of orientated bio-recognition elements (Liu et al., 2016).

We are presenting here the development of an AuNPs based SPRi biosensor for AFB_1 detection. To do so, chemically modified AuNPs were grafted over a SAM Au chip surface

through an amine linkage. Protein-A was used as an orientating immobilization tool of AFB_1 specific antibodies. For comparative study, bare Au sensor chips using the same immobilization protocol were used.

2. Experimental Section

2.1. Chemicals and Reagents

Anti-aflatoxin B_1 antibodies (anti-AFB_1) produced in rabbit, AFB_1 from Aspergillus flavus, α-Lipoic acid, cystamine dihydrochloride, Cetyltrimethylammonium bromide (CTAB), Dichloromethane (DCM), Sulphuric acid (H_2SO_4), Hydrogen Peroxide (H_2O_2), Chloroplatinic acid hydrate ($H_2PtCl_6.xH_2O$), Sodium Borohydride ($NaBH_4$), Gold(III) chloride hydrate ($HAuCl_4.xH_2O$), N-Ethyl-N'-(3-dimethylaminopropyl)carbodiimide hydrochloride (EDC), N-Hydroxy succinimide (NHS) were purchased from Sigma-Aldrich (France). Protein-A was obtained from RepliGen (USA). Phosphate Buffer Saline 10 mM pH 7.4 (PBS) tablets were supplied by Applichem (Germany). Other reagents were of analytical grade and used as such without further purifications. Milli-Q purified water (resistivity 18.2 MΩ cm) was used for the preparation of aqueous solutions.

2.2. Instruments

The optical measurement of synthesized nanomaterials as CTAB-AuNPs and Lipoic acid-AuNPs were performed with a UV-visible spectrometer (Jasco V-730) using quartz cuvette of 0.1 cm path length in the 300-800 nm range of wavelength, at room temperature. The surface morphology studies were carried out using a field emission gun Scanning Electron Microscope (SEM, MEB Quanta 250). X-ray diffraction patterns of AuNPs were measured on Rigaku X-ray diffractometer (2θ ranging from 10˚ to 80˚ consisting of Cu Kα radiation λ=0.154 nm), Transmission Electron Microscopy (TEM) images of as-prepared AuNPs were acquired with a Philips CM120 Microscope. Atomic Force Microscopy (Integra, NT-MDT) has been used to characterize SAM/Au chip and AuNPs/SAM/Au chip using Scanning probe microscope Solver PRO instrument in contact force mode with standard golden-silicon cantilevers. SPR measurements were performed using a 3-channel Kretschmann configuration (SPR-2, Sierra sensors, Hamburg, Germany) and a monochromatic *p*-polarized laser as the light source. In real time, the SPR angle shift (θ_{SPR}) was monitored through detecting changes in the intensity of reflected light with a photodiode detector. Sensor chips were a gold layer (□50 nm) coated glass prisms (Sierra sensors, Hamburg, Germany).

2.3. Synthesis of AuNPs and ligand exchange process (Figure 1, Step-1)

Colloidal AuNPs were synthesized using the seed-mediated method, slightly modified from the literature reported one (Fang et al., 2016). Briefly, 150 µL of 0.01 M $HAuCl_4.xH_2O$ and 100 µL of 0.01 M $H_2PtCl_6.xH_2O$ were added into 9.75 mL of 0.1 M CTAB solution followed by the drop by drop addition of 900 µL of ice-cold (4˚C) freshly prepared 0.01 M of $NaBH_4$ under constant magnetic stirring at room temperature. Thereby, the color of the resulting solution gradually changed from orange to colorless to light pink, indicates the formation of seed particles. The solution was left at room temperature for 4 hours in the dark to complete the reaction. The resulting solution was centrifuged at 4000 rpm for 10 minutes in order to remove excess solvent and the obtained pellet dispersed in distilled water. Afterward, stepwise replacement by ligand exchange method was carried out to replace CTAB surface ligands from as-prepared colloidal AuNPs to Lipoic acid using immiscible solvent DCM (Dewi et al., 2014). For this process, 5 mL of CTAB-AuNPs were mixed with 5 mL of DCM and kept at room temperature for 2 hours to allow separation of excess CTAB from upper phase (AuNPs in water) to bottom phase (DCM). Then, Lipoic acid (0.01 M) was added and kept reacting with AuNPs, in the dark for 4 hours at room temperature. Next, the resulting solution was centrifuged at 4000 rpm for 10 minutes in order to remove the excess of Lipoic acid.

For chemical conjugation of AuNPs with cystamine self-assembly modified SPRi chips, carboxylic functional groups from lipoic acid were activated in the presence of EDC 0.2 M and NHS 0.05 M, in the dark for 1 hour at room temperature (Bhardwaj et al., 2018).

2.4. Preparation of SPRi Au coated chip by Assembly of Monolayer (Figure 1, Step-2)

Au coated chips were cleaned with distilled water and rinsed with ethanol to remove any impurities. Subsequently, chips were treated with piranha solution (3:1 v/v of H_2SO_4 and H_2O_2) for 2 hours to remove all organic contaminations, washed with distilled water, rinsed with ethanol and dried under nitrogen (Torati et al., 2017). Clean chips were then functionalized in the presence of lipoic acid at a concentration of 10 mM in ethanol, at room temperature for 24 hours (Wang et al., 2014). Similarly, cystamine self-assembly was performed on clean chips in the presence of cystamine solution at a concentration of 0.01 M in distilled water for 24 hours (Xiao et al., 2014). Lipoic acid and cystamine SAM functionalized surfaces were finally rinsed with ethanol and distilled water, respectively, and dried under nitrogen. The obtained SAM/Au chips were stored for dry.

2.5. Deposition of Au NPs on SAM Au chip

EDC/NHS activated lipoic acid capped AuNPs (see 2.3) were poured on cystamine modified SPRi chip surface and stand to react for 12 hours in a humid chamber. Excess, unreacted AuNPs were washed out using distilled water. The obtained AuNPs/SAM/Au chips were stored for dry.

2.6. Modifications of SPRi chip for AFB_1 detection (Figure 1, Step-3)

Modifications of SPRi chip for AFB_1 detection were performed directly within the flow cell of the SPR-2 system. Briefly, SAM/Au and AuNPs/SAM/Au SPRi chips were loaded into the SPR-2 instrument and surface carboxylic acid groups activated in the presence of EDC 0.2 M and NHS 0.05 M, for 180 seconds at a flow rate of 25 µL/min. Then, protein-A was grafted on activated chip surface by injecting a solution of protein-A at a concentration of 200 µg/mL in pH 4.5 acetate buffer, for 180 seconds at a flow rate of 25 µL/min. The remaining activated carboxylic acid groups were then neutralized using ethanolamine (1 M in HCl pH 8.5), for 180 seconds at a flow rate of 25 µL/min.

Finally, anti-AFB_1 antibodies were immobilized by injecting anti-AFB_1 at a concentration of 100 µg/mL in phosphate buffer pH 7.4, for 180 seconds at a flow rate of 25 µL/min. Phosphate buffer (10 mM, pH 7.4) was used as running buffer for SPRi analysis. All the SPRi measurements were carried out at 25˚C.

2.7. Preparation of Real samples

Non-contaminated wheat samples were purchased from the local supermarket and solutions prepared using a previously reported method with slight modifications (Tralamazza et al., 2016). Briefly, 1 g of dry wheat was spiked with 200 µL of AFB_1 solutions (different concentrations were prepared in PBS, pH 7.4) and kept for 1 hour at room temperature. Then, 20 mL of 80/20 (v/v) methanol/water solution were added, stirred for 1 hour at room temperature and centrifuged at 5000 rpm for 10 minutes. The supernatant was carefully collected and diluted 1:5 with PBS. From this stock solution, 200 µL was used for further experimental analysis.

3. Results and Discussion

Synthesis of AuNPs, ligand exchange process and surface modification of multi-layered chips with and without AuNPs are depicted in **Figure 1**.

3.1. Structural and Microscopic analysis

Localized surface Plasmon resonance is highly dependent upon size, shape and chemical modification of nanoparticles. In order to characterize the optical plasmonic properties of our AuNPs, UV-visible absorbance spectroscopy studies were performed. **Figure S1(a, curve i)** presents UV-visible spectrum of synthesized CTAB-AuNPs in which a clear absorbance peak appeared at 528 nm, typical of the collective oscillation of electrons in the conduction band of AuNPs with specified incident wavelength (Ghasemi et al., 2015). Then, DCM washed AuNPs were characterized, and a similar absorbance peak at 528 nm was obtained (**Figure S1(a, curve ii)**), proof of the conservation of the colloidal behaviour of the DCM washed AuNPs. Finally, lipoic acid capped AuNPs were characterized through UV-visible spectrum analysis. As shown in **Figure S1(a, curve iii)**, a slight red shift of about 10 nm of the absorbance peak was observed, from 528 to 538 nm. This shift in absorbance peak was attributed to the electronic interaction between lipoic acid and the gold core of NPs (Dewi et al., 2014).

In order to determine the particular size and shape of synthesized NPs, TEM studies were carried out. **Figure 2(a)** depicts the TEM micrograph of freshly synthesized AuNPs. As a matter of fact, the obtained AuNPs were uniform spherical shaped, homogenous as well as well-dispersed with an approximate diameter of 20 nm. These spherical shapes of AuNPs were further confirmed by high-resolution TEM images (**Figure 2(b)**) together with their colloidal distribution in an aqueous medium.

X-ray diffraction patterns of AuNPs and SAM/Au, AuNPs/SAM/Au chip surfaces are shown in **Figure S1(b and c)**. Purity and crystallinity of AuNPs have been determined by XRD technique and their diffraction patterns are depicted in **Figure S1(b).** The primary diffraction peak of AuNPs appeared at 38.01˚ corresponds to (111) diffraction plane. The other peaks appeared at 47.11˚, 67.34˚ and 76.82˚ corresponds to (200), (220) and (311) diffraction planes, respectively. These peaks are indexed as the cubic structure of AuNPs with space group Fm3m (225) and matched with JCPDS file no. 04-0784 (Gautam et al., 2017).

Using Scherer Equation (1) (Holzwarth et al., 2011), we calculated the AuNPs average crystallite size,

$$\tau = 0.9\,\lambda/\beta\cos\theta \qquad (1)$$

Here, β is full width at half maximum (FWHM), λ is X-ray source wavelength (0.154 nm) for Cu Kα radiation. The average calculated crystallite size of AuNPs was then about 20 nm.

Further, XRD pattern of SAM/Au and AuNPs/SAM/Au surface were investigated by XRD technique. **Figure S1(c, curve ii)** presents diffraction pattern of amine-functionalized self-assembled Au surface. The primarily diffraction peak appeared at 38.18˚corresponds to (111) diffraction planes and rest of the appeared peaks in **curve (ii)** are corresponding to (200), (220) and (311) diffraction planes of Au surface. After the decoration of AuNPs on self-assembly Au surface, the four prominent peaks' intensity are increased compared to SAM/Au. Moreover, no further change in peak position and without appearance of extra peak confirms the decoration of AuNPs over the SAM/Au surface [**Figure S1(b, curve iii)]**. This study revealed that AuNPs are present on SAM/Au surface without changing the structure and composition of AuNPs.

As a complementary study, the surface morphology of AuNPs/SAM/Au was characterized through scanning electron microscopy (SEM). The scanning images presented in **Figure 2(c, d)** were observed at different magnification (50Kx, 100Kx). Surface modification with AuNPs clearly demonstrates well-distribution and regular arrangement of ordered structure on-chip substrate, providing a favorable environment for grafting of protein-A and immobilization of antibodies anti-AFB_1.

Topographic studies of modified surfaces as SAM/Au chip and AuNPs/SAM/Au chip have been investigated by Scanning Probe Microscope Solver PRO in contact force mode with standard golden-silicon CSG01 cantilevers having a normal spring constant; images are shown in **Figure S2(a, b)**. AFM image of the SAM/Au chip in **Figure S2(a)** showed smooth and clear film formation whereas, after AuNPs deposition, a clear roughness appears, directly correlated to the size of the particles (**Figure S2(b))** with no evidence of large aggregates.

3.2. Signal amplification study using AuNPs

To determine the impact of AuNPs on SPR chip surfaces AuNPs/SAM/Au and SAM/Au chips, gradient of NaCl concentration (from 0.5 to 7.5 % in distilled water) was used to perform the experiment at a flow rate of 25 µL/min. As can be seen in **Figure S3 (curve a and b)**, a clear difference of the sensor response was evidenced between the two studied surfaces with a dose-response. In the case of bare SAM/Au sensor chip, linear calibration curve was obtained with SPR signal as a function of NaCl concentration result shown in **Figure S3 (curve a)**. Linear regression parameter (R) was 0.98 whereas in another case of AuNPs/SAM/Au chip, linear calibration curve depicted in **Figure S3 (curve b)** and the linear regression coefficient of (R) was 0.97.

In a result, slope approximately 3-time higher (231.77 RU/% *vs.* 89.6 RU/%) when the chip surface was covered with AuNPs. This effect shall be attributed to the enhancement of plasmonic resonance coupling and electromagnetic coupling of Au sensing surface covered with AuNPs (Li et al., 2015). The sensitivity of the AuNPs/SAM/Au to mass variations on its surface during the subsequent experiments was then expected to be at least 3-time higher than on SAM/Au surface.

3.3. Preliminary *in-situ* SPRi studies of modified multilayered chip surfaces

Once the sensor surfaces prepared and characterized, all further modifications (**Step-3** of **Figure 1**) were performed *in-situ* within the SPRi microfluidic system. This approach permitted to advantageously follow these crucial surface modification steps through SPRi change measurements.

As a matter of fact, a clear difference one more time was observed between the two sensor surfaces **[Figure 3(a, b)]**. Indeed, even if in both cases, obvious evidence of the protein-A grafting and then the interaction of the anti-AFB_1 were obtained (increasing of signal related to mass deposition), the SPRi signals generated by each modification step were much stronger in the presence of AuNPs on the surface of the sensors. More precisely, a 3-time factor was here again obtained between antibodies immobilization signal on AuNPs/SAM/Au (7800 RU) and SAM/Au (2500 RU) **[Figure 3(b)]**.

3.4 SPRi-based AFB_1 detection

Finally, the impact of the presence of the AuNPs on the chip surface was studied through the use of the sensor for AFB_1 detection. SPRi based analysis was then performed using sensing layers prepared by either SAM/Au or AuNPs/SAM/Au surfaces.

Figure 4(a) presents the results obtained on anti-AFB_1/protein-A/AuNPs/SAM/Au chip surface. Various concentrations of AFB_1, from 0.01 to 50 nM, were injected in the system and the real-time SPRi response recorded. As can be observed from the calibration curve of **Figure 4(a)**, SPRi response signal increases as by increasing AFB_1 concentration due to the binding of AFB_1 molecules to immobilized anti-AFB_1 at the surface of the sensor. It has been reported that by increasing the concentration of analyte on the SPRi sensor chip surface, signals in term of response unit increases due to the binding of antigen and antibody (Park et al., 2014). Similarly, Majzik et al., also studied the interaction of AFB_1 to anti-AFB_1 biomolecules (Majzik et al., 2015). It has also been exposed that by increasing the AFB_1

concentration into the flow system, AFB_1 analyte bind with immobilized molecules over the sensor surface results to change in SPRi signal.

From the obtained dose-response calibration curve, a linear dependency was found with AFB_1 concentration ranging from 0.01 to 50 nM. Linear calibration curve was plotted between SPR response signal as a function of AFB_1 concentration and linear regression (R) parameter found was 0.99. A limit of detection of 0.003 nM was calculated using the following formula (2):

$$LOD = 3\sigma/m \quad (2)$$

where σ is the standard deviation of blank solution and m is the slope of the calibration curve. The sensitivity of anti-AFB_1/protein-A/AuNPs/SAM/Au immunoassay was found to be 75.43 RU/nM.

For control study, similar experiments were performed without AuNPs chip surface of anti-AFB_1/protein-A/SAM/Au [**Figure 4(b)**]. As by increasing the concentration of AFB_1 ranging from 1-100 nM corresponding SPRi response signal increased and linear dependency was found to be in the range of 1-50 nM **[Inset image: Figure 4(b)**]. From the calibration curve, linear regression coefficient (R) value found to 0.97. A limit of detection of only 0.19 nM was found this time with a sensitivity of the analytical system of 15.72 RU/nM.

As a result, even if both surfaces were able to detect $aAFB_1$, the AuNPs/SAM/Au-based system prove itself to be 3-time more sensitive than the SAM/Au-based one, leading to a 6-time lower limit of detection.

To view the mechanistic insight on the effect of variation of antigen concentration, SAM-protein A provides flexible anchor and directional orientation to immobilize anti-AFB_1 biomolecules on sensor chip surface that allow easy antigen-antibody interaction. Also, by continuous flow of sample on sensor chip, the change in SPRi sensing signal is observed due to the binding of analyte to covalently immobilized biomolecules (Mullett et al., 2000).

The present study demonstrated that required signal amplification for small molecules AFB_1 detection has been achieved using the functionalized AuNPs-based sensor chip. Surface morphology by AuNPs influences the field environment by LSPR-SPR coupling effect between AuNPs and Au film substrate (Szunerits et al., 2014). **Table 2** summarizes the comparison of previously reported SPR and SPRi based AFB_1 sensors with the present work. Noticeably, important biosensing characteristics have been enhanced using our AuNPs-based SPRi. Low LOD in a wide range of detection demonstrate a promising approach for fast, reliable, sensitive monitoring of mycotoxin.

3.5 Analysis in spiked Wheat samples

In order to validate the performances of the developed immunosensor for AFB_1 detection, real sample studies were carried out using contaminated wheat samples. In this study, various wheat samples were spiked with known concentrations of AFB_1 and analyzed using the optimized AuNPs/SAM/Au-based SPRi system. Details of this experiment are described in the experimental 2.6 section. **Table 1** presents the analytical results obtained. As can be seen, the recovery responses of the different AFB_1 concentrations were found to be 93% and 90.1%, for 0.1 nM and 1 nM, respectively.

Conclusions

A label-free optical SPR-based ultrasensitive immunosensor was developed for AFB_1 detection commonly found in food. Using AuNPs on the sensor chip surface that act as signal amplifier and provides a large surface for the immobilization of anti-AFB_1 antibodies. AuNPs integrated immunosensor respond linearly with various AFB_1 antigen concentration in the detection range from 0.01 to 50 nM with a limit of detection of 0.003 nM. Whereas, bare SAM sensor chip surface showed linear SPR response signal with AFB_1 antigen concentration ranging from 1 to 50 nM and detection limit was 0.19 nM. Thus, AuNPs integrated sensor chip surface AuNPs/SAM/Au system was three-time more sensitive (75.43 RU/nM) than bare SAM/Au sensor chip (15.72 RU/nM), leading to the 6-time lower limit of detection. Thus, in-spite of a standard detection system for AFB_1, real sample analysis was performed using contaminated wheat samples with various spiked AFB_1 antigen concentration and average percentage recoveries found to be acceptable (93 and 90.1%). This SPR based biosensor showed great potential to detect other small molecules of mycotoxins using their respective biorecognition element on the same platform matrix.

Declaration of Interest

The Authors declare that there is no conflict of interest.

Acknowledgments

H.B. acknowledges to Indo-French Center for the Promotion of Advanced Research (IFCPAR/CEFIPRA) for the financial support.

References

Bhardwaj, H., Singh, C., Kotnala, R. K., & Sumana, G. (2018). Graphene quantum dots-based nano-biointerface platform for food toxin detection. *Analytical and bioanalytical chemistry*, *410*(28), 7313-7323. DOI: 10.1007/s00216-018-1341-y

Devi, R. V., Doble, M., & Verma, R. S. (2015). Nanomaterials for early detection of cancer biomarker with special emphasis on gold nanoparticles in immunoassays/sensors. *Biosensors and Bioelectronics*, *68*, 688-698. DOI: 10.1016/j.bios.2015.01.066

Dewi, M. R., Laufersky, G., & Nann, T. (2014). A highly efficient ligand exchange reaction on gold nanoparticles: preserving their size, shape and colloidal stability. *RSC Advances*, *4*(64), 34217-34220. DOI: 10.1039/c4ra05035e

Fang, C., Zhao, G., Xiao, Y., Zhao, J., Zhang, Z., & Geng, B. (2016). Facile growth of high-yield gold nanobipyramids induced by chloroplatinic acid for high refractive index sensing properties. *Scientific reports*, *6*, 36706. DOI: 10.1038/srep36706

Gautam, P. K., Kumar, S., Tomar, M. S., Singh, R. K., & Acharya, A. (2017). Biologically Synthesized Gold Nanoparticles using Ocimum sanctum (Tulsi Leaf Extract) Induced Anti-Tumor Response in a T Cell Daltons Lymphoma. *J Cell Sci Ther*, *8*(278), 2. DOI: 10.4172/2157-7013. 1000278

Ghasemi, F., Hormozi-Nezhad, M. R., & Mahmoudi, M. (2015). A colorimetric sensor array for detection and discrimination of biothiols based on aggregation of gold nanoparticles. *Analytica chimica acta*, *882*, 58-67. DOI: 10.1016/j.aca.2015.04.011

Goyal, S., Ramawat, K. G., & Merillon, J.-M. (2016). Different shades of fungal metabolites: an overview. *Fungal Metabolites*, 1-29. DOI: 10.1007/978-3-319-19456-1_34-1

Heshmati, A., Zohrevand, T., Khaneghah, A. M., Nejad, A. S. M., & Sant'Ana, A. S. (2017). Co-occurrence of aflatoxins and ochratoxin A in dried fruits in Iran: Dietary exposure risk assessment. *Food and chemical toxicology*, *106*, 202-208. DOI: 10.1016/j.fct.2017.05.046

Holzwarth, U., & Gibson, N. (2011). The Scherrer equation versus the 'Debye-Scherrer equation'. *Nature nanotechnology*, *6*(9), 534. DOI: 10.1038/nnano.2011.145

Jia, Y., Peng, Y., Bai, J., Zhang, X., Cui, Y., Ning, B., Cui, J., & Gao, Z. (2018). Magnetic nanoparticle enhanced surface plasmon resonance sensor for estradiol analysis. *Sensors and Actuators B: Chemical*, *254*, 629-635. DOI: 10.1016/j.snb.2017.07.061

Joshi, S., Segarra-Fas, A., Peters, J., Zuilhof, H., van Beek, T. A., & Nielen, M. W. F. (2016). Multiplex surface plasmon resonance biosensing and its transferability towards imaging

nanoplasmonics for detection of mycotoxins in barley. *Analyst*, *141*(4), 1307-1318. DOI: 10.1039/c5an02512e

Kensler, T. W., & Groopman, J. D. (2018). Aflatoxin Exposure, Human Liver Cancer Risk, and Chemoprevention. *Carcinogens, DNA Damage And Cancer Risk: Mechanisms Of Chemical Carcinogenesis*, 143. DOI: 10.1142/9789813237209_0006

Koedrith, P., Thasiphu, T., Weon, J.-I., Boonprasert, R., Tuitemwong, K., & Tuitemwong, P. (2015). Recent trends in rapid environmental monitoring of pathogens and toxicants: potential of nanoparticle-based biosensor and applications. *The Scientific World Journal*, *2015*. DOI: 10.1155/2015/510982

Li, A., Isaacs, S., Abdulhalim, I., & Li, S. (2015). Ultrahigh enhancement of electromagnetic fields by exciting localized with extended surface plasmons. *The Journal of Physical Chemistry C*, *119*(33), 19382-19389. DOI: 10.1021/acs.jpcc.5b05830

Liu, Y., & Yu, J. (2016). Oriented immobilization of proteins on solid supports for use in biosensors and biochips: a review. *Microchimica Acta*, *183*(1), 1-19. DOI: 10.1007/s00604-015-1623-4

Majzik, A., Hornok, V., Sebok, D. n., Bartok, T., Szente, L., Tuza, K., & Dekany, I. (2015). *Sensitive Detection of Aflatoxin B1 Molecules on Gold SPR Chip Surface Using Functionalized Gold Nanoparticles*. DOI: 10.1556/0806.43.2015.3.8

Martinsson, E., Sepulveda, B., Chen, P., Elfwing, A., Liedberg, B., & Aili, D. (2014). Optimizing the refractive index sensitivity of plasmonically coupled gold nanoparticles. *Plasmonics*, *9*(4), 773-780. DOI: 10.1007/s11468-013-9659-y

Mateo, E. M., Gomez, J. V., Romera, D., Tarazona, A., Gimeno-Adelantado, J. V., Mateo-Castro, R., & Jimenez, M. (2018). Environmental Temperature and Relative Humidity, two Key Factors in Maize Technology Affecting Ochratoxin a Production and Growth of Ochratoxigenic Species. *International Journal of Food Engineering*, *4*(1). DOI: 10.18178/ijfe.4.1.51-57

Moon, J., Byun, J., Kim, H., Lim, E.-K., Jeong, J., Jung, J., & Kang, T. (2018). On-site detection of aflatoxin B1 in grains by a palm-sized surface plasmon resonance sensor. *Sensors*, *18*(2), 598. DOI: 10.3390/s18020598

Mullett, W. M., Lai, E. P. C., & Yeung, J. M. (2000). Surface plasmon resonance-based immunoassays. *Methods*, *22*(1), 77-91. DOI: 10.1006/meth.2000.1039

Negash, D. (2018). A review of aflatoxin: occurrence, prevention, and gaps in both food and feed safety. *Journal of Applied Microbiological Research*, *1*, 35-43.

Nikolovska-Coleska, Z. (2015). Studying protein-protein interactions using surface plasmon resonance. *Protein-Protein Interactions* (pp. 109-138): Springer. DOI: 10.1007/978-1-4939-2425-7_7

Omrani, N. M., Hayat, A., Korri-Youssoufi, H., & Marty, J. L. (2016). Electrochemical biosensors for food security: Mycotoxins detection. *Biosensors for Security and Bioterrorism Applications* (pp. 469-490): Springer. DOI: 10.1007/978-3-319-28926-7_22

Park, J. H., Kim, Y.-P., Kim, I.-H., & Ko, S. (2014). Rapid detection of aflatoxin B1 by a bifunctional protein crosslinker-based surface plasmon resonance biosensor. *Food Control*, *36*(1), 183-190. DOI: 10.1016/j.foodcont.2013.08.038

Richard, J. L. (2007). Some major mycotoxins and their mycotoxicosis-An overview. *International journal of food microbiology*, *119*(1-2), 3-10. DOI: 10.1016/j.ijfoodmicro.2007.07.019

Sun, L., Wu, L., & Zhao, Q. (2017). Aptamer based surface plasmon resonance sensor for aflatoxin B1. *Microchimica Acta*, *184*(8), 2605-2610. DOI: 10.1007/s00604-017-2265-5

Szunerits, S., Spadavecchia, J., & Boukherroub, R. (2014). Surface plasmon resonance: signal amplification using colloidal gold nanoparticles for enhanced sensitivity. *Reviews in Analytical Chemistry*, *33*(3), 153-164. DOI: 10.1515/revac-2014-0011

Torati, S. R., Kasturi, K. C. S. B., Lim, B., & Kim, C. (2017). Hierarchical gold nanostructures modified electrode for electrochemical detection of cancer antigen CA125. *Sensors and Actuators B: Chemical*, *243*, 64-71. DOI: 10.1016/j.snb.2016.11.127

Tralamazza, S. M., Bemvenuti, R. H., Zorzete, P. c., de Souza Garcia, F. b., & Correa, B. (2016). Fungal diversity and natural occurrence of deoxynivalenol and zearalenone in freshly harvested wheat grains from Brazil. *Food chemistry*, *196*, 445-450. DOI: 10.1016/j.foodchem.2015.09.063

Tsekenis, G., Chatzipetrou, M., Massaouti, M., & Zergioti, I. (2019). Comparative Assessment of Affinity-Based Techniques for Oriented Antibody Immobilization towards Immunosensor Performance Optimization. *Journal of Sensors*, *2019*. DOI: 10.1155/2019/6754398

Wang, X., Ju, J., Li, J., Li, J., Qian, Q., Mao, C., & Shen, J. (2014). Preparation of electrochemical cytosensor for sensitive detection of HeLa cells based on self-assembled monolayer. *Electrochimica Acta*, *123*, 511-517. DOI: 10.1016/j.electacta.2014.01.027

Wang, X., Shan, Y., Gong, M., Jin, X., Jiang, M., & Xu, J. (2019). A novel electrochemical sensor for ochratoxin A based on the hairpin aptamer and double report DNA via multiple

signal amplification strategy. *Sensors and Actuators B: Chemical*, *281*, 595-601. DOI: 10.1016/j.snb.2018.10.148

Xiao, X., Ulstrup, J., Li, H., Zhang, J., & Si, P. (2014). Nanoporous gold assembly of glucose oxidase for electrochemical biosensing. *Electrochimica Acta*, *130*, 559-567. DOI: 10.1016/j.electacta.2014.02.146

Zhang, Z., Yu, L., Xu, L., Hu, X., Li, P., Zhang, Q., Ding, X., & Feng, X. (2014). Biotoxin sensing in food and environment via microchip. *Electrophoresis*, *35*(11), 1547-1559. DOI: 10.1002/elps.201300570

A Label-Free Ultrasensitive Microfluidic Surface Plasmon Resonance Biosensor for Aflatoxin B_1 detection using Nanoparticles integrated Gold chip

Hema Bhardwaj[a,b,c], Gajjala Sumana[b,c], Christophe A. Marquette[a*]

[a]Institute for Molecular and Supramolecular Chemistry and Biochemistry (ICBMS), University Claude Bernard Lyon 1, Villeurbanne Cedex-69100, France
[b]Academy of Scientific and Innovative Research (AcSIR), Ghaziabad-201002, India
[c]Biomedical Metrology Section, CSIR-National Physical Laboratory, Dr. K.S. Krishnan Marg, New Delhi-110012, India

Figure 1: Schematic illustration of the different steps involved in the biosensor active surface modification. **Step-1**: Synthesis of AuNPs and ligand exchange process from CTAB to lipoic acid surface modification. **Step-2**: Self-assembled monolayer of cystamine and lipoic acid on Au sensor chips surface. **Step-3**: *in-situ* activation of SAM-modified chip surface, grafting of protein-A and immobilization of anti-AFB_1 antibodies followed by interaction with AFB_1 antigen.

Figure 2: (a, b) Transmission Electron Microscopy (TEM) images of as-synthesized AuNPs at different magnification scales, (c, d) Scanning Electron Microscopy (SEM) images of AuNPs on the gold chip surface.

Figure 3 (a, b) presents the SPRi signal variations obtained during (a, a') surface activation with EDC-NHS, (b, b') protein-A grafting, (c, c') surface saturation using ethanolamine and (d, d') anti-AFB_1 orientated immobilization. During these experiments, channel 1 and channel 2 of the apparatus were used as control and assay, respectively. The control experiment surface being identical to the assay one, only lacking the anti-AFB_1 immobilization (d, d').

Figure 4 (a) Calibration plot of SPR response signal obtained with aAFB_1/protein-A/SAM/Au fabricated SPR chip as a log function of AFB_1 concentration (1.0, 5.0, 10, 50, 100 nM [Inset image: Linear calibration plot of variation of SPR response signal with AFB_1 concentration], (b) Linear calibration plot of SPR response signal varied with Log of concentration of AFB1 (0.01, 0.05, 0.1, 0.5, 1.0, 5.0, 10, 50 nM).

Table 1: Analytical results of AFB_1 detection in wheat samples using the fabricated sensor.

Table 2: Comparison table of reported SPR and SPRi biosensor for AFB_1 detection with present work.

Figure 1:

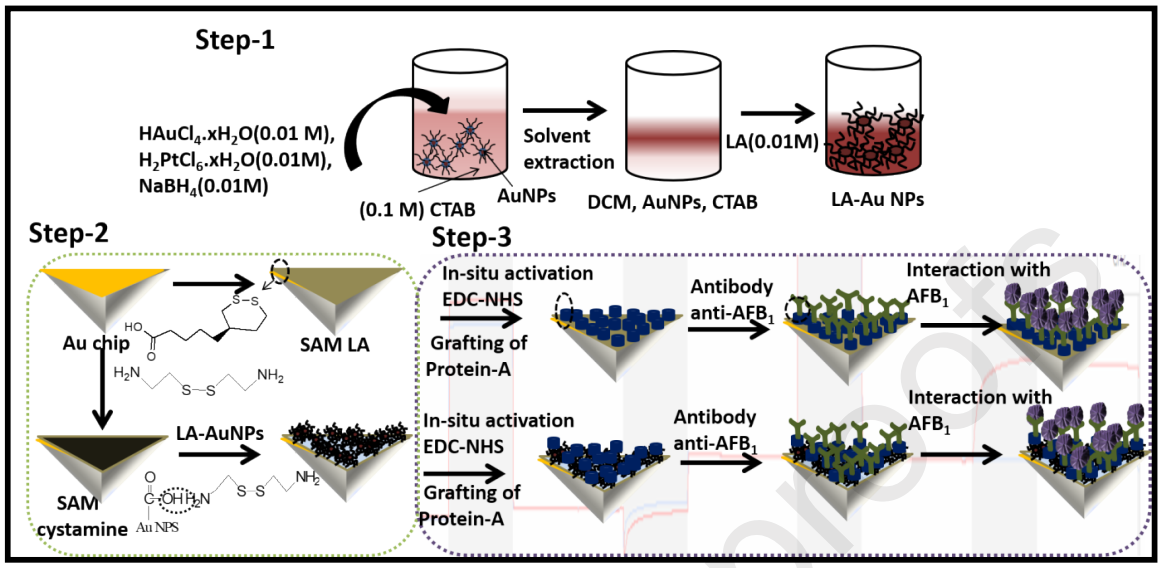

Figure 2:

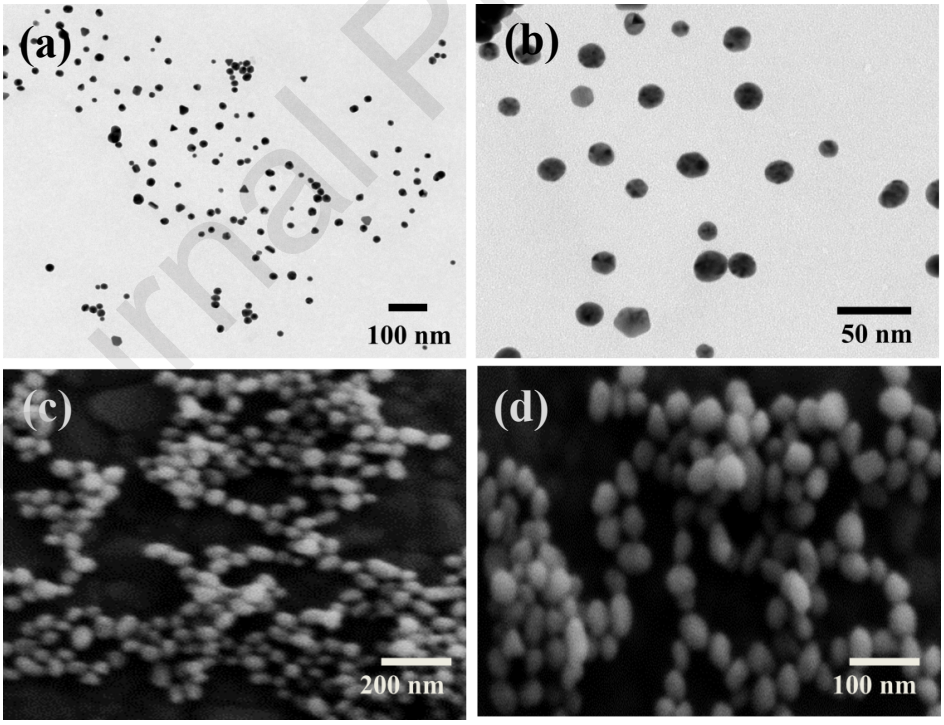

Figure 3:

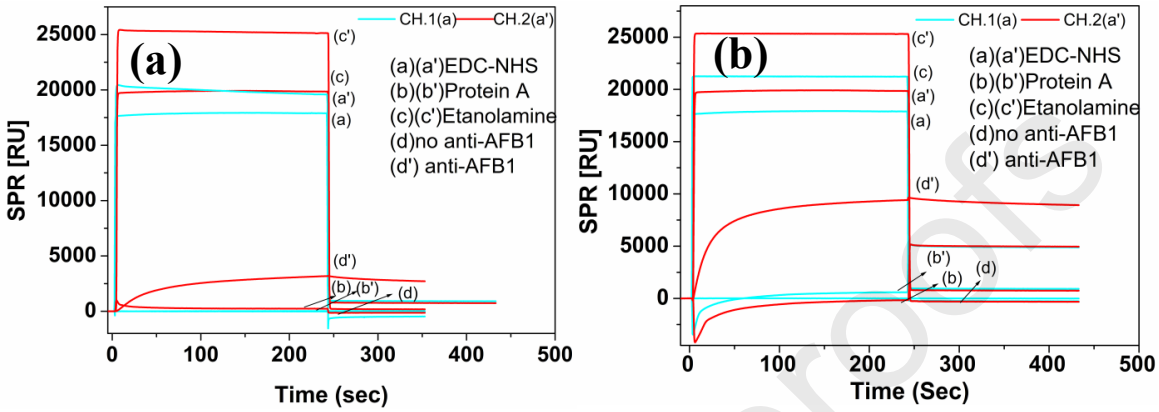

Figure 4:

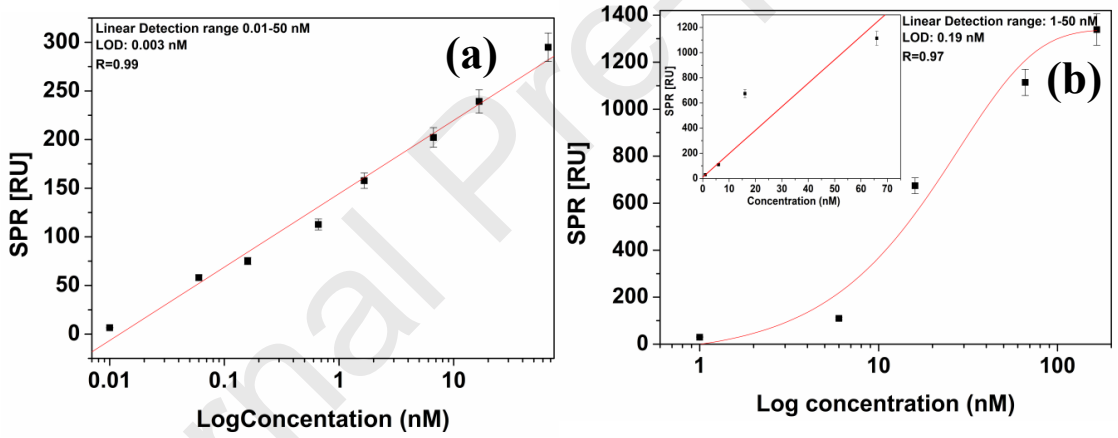

Table 1:

Non-contaminated samples	S. No.	Spiked concentration (nM)	Experimental found concentration (nM)	Absolute Recovery (%)
Wheat	1.	0 (Blank)	0	-
	2.	0.1	0.093	93
	3.	1.0	0.901	90.1

Table 2:

S.No.	Immunoassay	Detection Technique	Detection range of AFB_1	Limit of detection	References
1.	SAM* aminothiol	SPR*	0.5-100 µg/mL	1 µg/mL	Park et al., 2014
2.	Au chip	SPR	16-20 ppb	2.5 ppb or ng/mL	Moon et al., 2018
3.	AuNPs* β-cyclodextrin	SPR	0.01-23.6 ng/mL	1 pg/mL	Majzik et al., 2015
4.	Aptamer based Au chip	SPR	0.4-200 nM	0.4 nM	Sun et al., 2017
5.	PEG*/Au nanostructured	SPRi*	3-260 µg/kg	0.6 µg/kg	Joshi et al.,
6.	AuNPs/SAM/Au chip	SPRi	0.01-66.6 nM	0.003 nM	Present work
	SAM/Au chip	SPRi	1-66 nM	0.19 nM	

*SAM-self assembled monolayer, *SPR-Surface Plasmon Resonance, *AuNPs-Gold nanoparticles, *PEG-polyethylene Glycol, SPRi-Surface Plasmon Resonance imaging

Declaration of interests

☒ The authors declare that they have no known competing financial interests or personal relationships that could have appeared to influence the work reported in this paper.

☐The authors declare the following financial interests/personal relationships which may be considered as potential competing interests:

Highlights

1. Successfully synthesized CTAB-AuNPs using chemical reduction process.
2. Ligand exchange method was adopted to functionalized Lipoic acid AuNPs.
3. Comparative SPR studies performed on multi-layered Au chip sensing substrate.
4. Decorated AuNPs chip surface shows high sensitivity, low LOD for AFB_1 detection.
5. Validation of the proposed biosensor was evaluated by spiked wheat samples.